

Mom and Baby Wellness with a Smart Lactation Pad: A Wearable Sensor-Embedded Lactation Pad for on-Body Quantification of Glucose in Breast Milk

Abdulrahman Al-Shami, Haozheng Ma, Melissa Banks, Farbod Amirghasemi, Mona A Mohamed, Ali Soleimani, Sina Khazaee Nejad, Victor Ong, Alessandro Tasso, Alara Berkmen, and Maral P. S. Mousavi*

Wearable sensors are transforming healthcare by facilitating rapid, non-invasive, on-body biochemical analysis in biofluids such as sweat, tears, saliva, and blood, providing real-time insights into health conditions. Despite extensive academic and industrial efforts in developing wearable devices, very few are tailored to meet women's health needs. None are specifically designed for measurements in human breast milk. Beyond being the optimal source of infant nutrition, milk serves as a rich biofluid containing potential biomarkers reflecting a mother's health as well. Analyzing the composition of milk offers valuable information for the health of the infant, and the mother. This work pioneers a wearable sensor embedded in a lactation pad for on-body sampling of breast milk and continuous analysis of glucose levels in breast milk. Lactation pads are worn by most lactating individuals to absorb milk leakage during the day, and keep the cloth dry. In this work, by integrating microfluidic channels and electrochemical sensors in the lactation pad, milk sampling and analysis becomes part of an existing daily routine for the mother, posing no additional burden for milk sampling and analysis. The electrochemical sensors are developed using laser-induced carbonization of polyimide thin films, allowing for development of flexible, low-cost, and high-surface area electrodes. Glucose sensing is done via an enzymatic membrane composed of glucose oxidase, glutaraldehyde, bovine serum albumin, and Nafion to achieve enhanced enzyme protection and extended biosensor shelf life and operation in milk. Notably, the wearable device demonstrates high accuracy (96.8 to 104.1%) in measurement of glucose in whole undiluted human milk, collected 1st, 6th, and 12th months postpartum. This innovative smart lactation pad empowers mothers to track their babies' glucose intake and potentially identify early signs of health concerns.

1. Introduction

The correlation between our health and food has been recognized since ancient times.^[1–3] Food is our energy source for survival, but the quality and composition of that food significantly impacts our body's ability to function in both a physical and cognitive capacity.^[4–7] Healthy food helps maintain organ function, supports the immune system, and regulates mood,^[8–10] whereas unhealthy food choices can significantly increase the risk of a wide range of physical problems and mental health disorders.^[11–20] Nowadays, people commonly monitor their diets using nutrition labels or apps that track calorie and nutrient intake. However, similar tools for detailed analysis of human breast milk, the sole source of neonatal nutrition, remain unavailable. Breast milk is the ideal infant nutrition source, supporting physical, cognitive, and behavioral development.^[21–25] It also provides protection against acute and chronic conditions, including sudden infant death syndrome (SIDS), asthma, and obesity.^[26,27] However, its composition can change significantly due to the nutritional status of the lactating individual or metabolic disorders, potentially affecting infant growth and development.^[28–30]

Research on developing tools for at-home or on-body biochemical analysis is limited. Currently, there are no wearable platforms designed for chemical analysis of breast

A. Al-Shami, H. Ma, M. Banks, F. Amirghasemi, M. A Mohamed, A. Soleimani, S. Khazaee Nejad, V. Ong, A. Tasso, A. Berkmen, M. P. S. Mousavi
 Alfred E. Mann Department of Biomedical Engineering
 University of Southern California
 1042 Downey Way, Los Angeles, CA 90089, USA
 E-mail: mousavi.maral@usc.edu

milk, and there is only a small amount of work focusing on point-of-care analysis in this area. A few products and services for biochemical analysis of breast milk have recently been introduced to assist with management of breastfeeding (Table 1). In 2018 the U.S. Food and Drug Administration (FDA) authorized the Miris Human Milk Analyzer for use in hospital settings to quantify breast milk nutrients.^[31] This instrument uses infrared analyzers and is bulky (bench-top), expensive, and requires skilled operators for proper analysis. Consequently, accessibility for

 The ORCID identification number(s) for the author(s) of this article can be found under <https://doi.org/10.1002/adfm.202420973>
 DOI: 10.1002/adfm.202420973

Table 1. Comparison between existing devices (labeled with 1) and services (labeled with 2) for biochemical analysis in milk with the wearable sensor developed in this work. NR stands for not reported.

	This Work ¹	Alcohol Test Strips ¹	Lactation Lab (premium kit) ²	Milkify ²	Creatomatcrit Plus Analyzer ¹	Miris HMA Analyzer ¹
Device or Service Description	Sensor-embedded lactation pad for on-body milk sampling and continuous analysis	Test strips dipped into human milk	Milk is sampled at home and shipped for analysis	Milk is sampled at home and shipped for analysis	Separates fatty and non-fatty content from milk and estimates energy and fat percentage	Milk is injected in the device for analysis in a laboratory
At-home Analysis	Yes	Yes	No	No	No	No
Cost	~\$0.5	~\$1.0	\$349	\$200	\$800	\$5000
Wearable	Yes	No	No	No	No	No
On-body Milk Sampling	Yes	No	No	No	No	No
Continuous Analysis	Yes	No	No	No	No	No
Detected Analytes	Glucose (can be expanded by changing electrode surface functionalization)	Alcohol	Energy, fat, minerals, heavy metals, carbohydrates, protein, and vitamins	Energy, proteins, fats, and carbohydrates	Fat and energy	Energy, fat, and protein content
Method of Analysis	Electrochemical	Colorimetric	NR	NR	Centrifuge Separation	Mid-infrared Spectroscopy
Sample Volume	400 μL	NR	60 mL	NR	NR	3 mL
Sample Processing	No	No	NR	Freeze-Drying	Centrifuge	Sonication and heating
Time to Results	2 minutes	2 minutes	1 week	1-3 weeks	30 minutes (sample processing factored in)	30 minute (sample processing factored in)

parents in a home setting is limited and use is generally restricted to hospital laboratories and milk banks.^[32] An alternative approach to analysis is the use of commercial mail-in services offering nutrient quantification. These services typically require sample collection using specialized kits and shipment to company laboratories for analysis and range in cost from \$49–\$349,^[33,34] which poses logistical hurdles as well as delays results. The only low-cost test for rapid at-home analysis in breast milk are commercially available alcohol test strips (alcohol can impair infant's development, growth, and circadian rhythm,^[35–38] and milk containing alcohol should be discarded). Table 1 summarizes the commercially available devices for human milk analysis compared to the device developed in this work.

The state-of-the-art tools pose numerous challenges for obtaining useful information through the analysis of breast milk. The expensive mail-in-kits only allow limited number of testings (depending on what the parents can afford) and provide the results with several weeks of delay. The composition of breast milk changes over time to accommodate the needs of a growing child, and is also dependent on the mother's diet,^[39] therefore frequent analysis is needed to obtain actionable and relevant information on milk content. Another challenge is practicality: new parents are often very busy and may lack the time to research testing facilities and collect samples for mail-in services. For breast milk collection and analysis to be practical for busy families, it must be quick, affordable, discreet, and easy to use.

Lactating individuals face unique health concerns such as nutritional deficiencies, mastitis development, and drug transfer-

ence through their milk. Therefore, it seems only natural to take advantage of a freely-available, non-invasive biofluid to help these individuals monitor the health of themselves and their child. The introduction of accessible, home-based wearable devices for breast milk analysis has the potential to revolutionize the breastfeeding experience. Such devices could empower families with immediate data, offering a safe and well-monitored breastfeeding journey that prioritizes infant nutrition and maternal health. In recent years, we have seen an explosion of wearable technologies such as smart watches, bracelets, armbands, and glasses, and these tools are becoming a part of people's daily lives.^[40–44] Wearable devices have greatly improved the healthcare system by reducing the burden on hospitals and providing reliable information for disease diagnosis and therapeutic monitoring.^[45–53] Moreover, the non-invasive nature of wearable devices has simplified diagnostic procedures and reduced the risk of infection, previously associated with blood-related interventions.^[54,55] Various wearable devices are integrated with sampling and sensing platforms to analyze different chemical and biological markers for healthcare applications.^[45,56–59] Those wearables are developed to perform biochemical measurements in different biofluids, i.e., saliva, urine, sweat, etc. and can be worn on various body parts, e.g., eye, head, wrist, fingers, etc. to assist in health monitoring of medical testing.^[59–66] The field of women's health, however, has been largely excluded from these advancements. This is particularly troubling given our lack of understanding of the makeup of human breast milk and daily changes of its biochemical composition. Wearable sensors for point-of-care and at-home

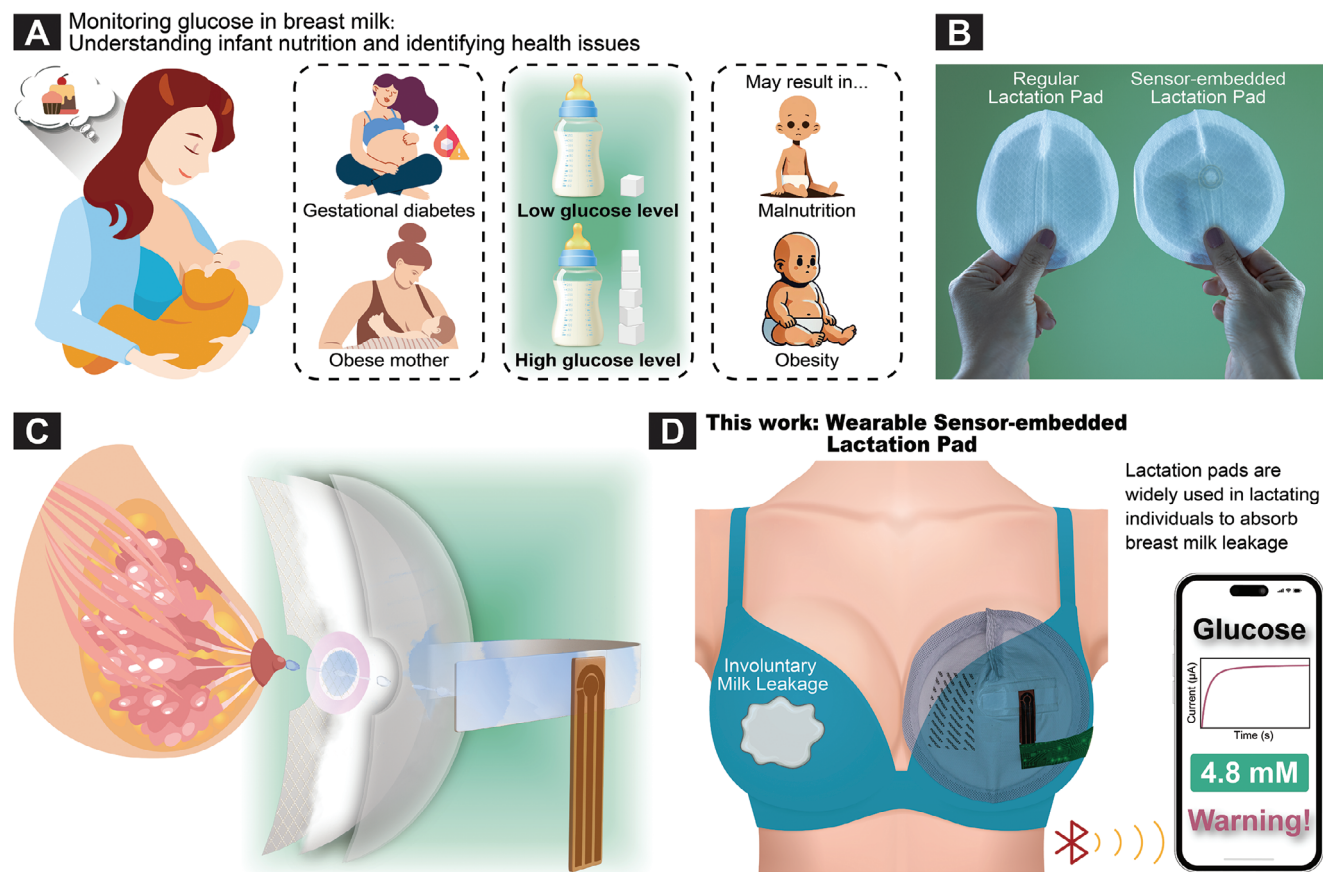


Figure 1. Overview of the developed wearable device. A) The importance of monitoring of glucose in breast milk due to potential impact of hypoglycemia and hyperglycemia on infant health. B) Real photo of commercial regular lactation pad and sensor-embedded lactation pad. Lactation pads are widely used by lactating individuals to absorb breast milk leakage and keep the cloth dry. C) The layer-by-layer exploded structure of the smart lactation bra pad with embedded microfluidic channels and electrochemical sensors for on-body milk sampling and glucose sensing. D) The smart lactation pad is used similar to a regular lactation pad. The biochemical analysis and data transfer are achieved using a flexible potentiostat secured on the pad (not developed in this work). The milk stain on the left breast shows the common problem of involuntary milk leakage during lactation.

testing of milk will be an ideal solution for frequent monitoring of milk composition.

This work pioneers the first wearable sensor capable of biochemical measurements in breast milk. Our wearable sensor is embedded into a lactation pad for on-body milk collection, and analysis, use with no additional burden of testing (Figure 1). Lactation pads (also known as nursing pads or nursing bra pads) are worn inside a bra to absorb breast milk leakage in order to keep the bra and clothing dry (Figure 1B). The underlying cause of leakage in lactation is the subject of continued debate, and milk can leak through one or multiple of the following reasons: (1) oversupply of milk in the breasts, (2) the unexpected let-down reflex from environmental stimulation (such as hearing an infant cry), and (3) changes in the breastfeeding schedules.^[67] Breast milk leakage rates vary, but still range from a few milliliters to tens of milliliters per day,^[68–70] which is absorbed by the lactation pad and then discarded. We have incorporated microfluidic channels in a lactation pad to capture some leaked milk, and direct it to a sensing zone. The volume of milk leaked is sufficient for a wide range of biochemical analyses. We believe that nursing bra pads could serve as an innovative disposable wearable platform to analyze human milk directly from the breast. Such a device

provides parents and healthcare professionals with personalized assessments of maternal health status and infant nutritional patterns. Also, the non-invasiveness of this approach increases its accessibility to a wide range of breastfeeding individuals, providing them with the necessary information to promote the long-term health and well-being of both mother and child.

Our smart lactation pad is a platform device capable of on-body sampling of breast milk in a wearable device, and directing that milk to an electrochemical sensing zone that can be customized to measure a wide range of biomarkers. Specifically, we have integrated a glucose electrochemical sensing zone into the wearable smart-lactation pad, allowing for either continuous or frequent monitoring of glucose levels in breast milk. This glucose sensing zone utilizes glucose oxidase (GOx) as the biorecognition element, and prussian blue (PB) as a mediator. Electrochemical glucose enzymatic sensors are widely used for glucose monitoring due to their high sensitivity and specificity. In these sensors, GOx catalyzes glucose oxidation, generating hydrogen peroxide as a byproduct.^[71,72] PB is often employed as a redox mediator in these sensors, efficiently catalyzing the reduction of hydrogen peroxide at low potentials, minimizing interference from other substances.^[71,73] Enzymatic membranes are used to

immobilize GOx to enhance selectivity and extend the sensor's lifespan, providing a stable microenvironment that protects the enzyme and reduces fouling.^[74,75] This combination of PB and enzymatic membranes results in reliable and long-lasting glucose sensors suitable for various applications.

Glucose in breast milk is one of the most important nutrients to support a child's growth and aids in the brain development of the infant (Figure 1A).^[23,76] Maternal conditions like obesity and gestational diabetes influence glucose levels, with higher levels linked to obesity risks in infants, and lower levels potentially causing hypoglycemia in infants of diabetic mothers.^[77–79] Hypoglycemia, which can be asymptomatic, may affect neurodevelopment and requires careful monitoring.^[76,80–83] While links between maternal health, milk composition, and infant outcomes are still under investigation, monitoring breast milk glucose offers valuable insights. This work introduces tools for at-home milk analysis to advance maternal and infant health research. It is important to emphasize that any clinical interventions should be determined in consultation with the user's healthcare team and pediatrician, as the data and device readings are not intended for independent interpretation by the user. By integrating the proposed device with telehealth services or other healthcare provider options, a more holistic and effective approach to maternal and infant health can be achieved. This integration not only alleviates stress and anxiety for users but also preserves the empowering benefits of home-based monitoring.

2. Results and Discussion

2.1. Overview of the Wearable Platform

Nursing bra pads (Figure 1B) or lactation pads are commonly used by breastfeeding individuals to absorb milk leakage, protect the clothing from stains, and maintain comfort and hygiene throughout the day. In this work, we have taken advantage of this existing routine for lactating mothers, and incorporated a milk sampling and sensing capability to the lactation pad, to create a wearable device for on-body milk analysis (Figure 1C). The smart lactation pad developed in this work contains an absorbent material, similar to a standard nursing pad, and captures excess leaked milk to maintain the primary function of a nursing pad. The use of this wearable device is similar to the regular lactation pad (place the pad over the breast, the absorbing material in the pad will absorb the leaked milk), posing no additional burden on the already busy parent. A portion of the leaked milk is wicked into a microfluidic channel that has an inlet at the center of the bra pad (close to mammary papilla). This microfluidic channel directs the milk to a sensing zone for electrochemical analysis. The outlet of this milk sampling channel is connected to the absorbing material, where this material works as a fluidic sink to pull the fluid and refresh the channel with new milk (Figure 1C), allowing for continuous measurement during the day.

Figure 2 shows the fabrication and components of the smart lactation pad. Front and back of the wearable device is shown in Figure 2B,C. The skin interfacing side of the device is soft and comfortable against skin. A hydrophobic ring separates (3 in Figure 2B) the general milk absorbing zone from the microfluidic channel (cellulose paper) for milk sampling, and avoids contamination by the absorbing material for the milk that is directed

to the sensing zone. The electrochemical sensors are fabricated using laser-engraving (Figure 2D) to ensure low-cost of the sensors while maintaining high mechanical stability and flexibility for the sensors (important as bra pads are pressed to conform to the body shape, subjecting the sensors to mechanical stress). The laser-induced graphene (LIG) electrodes are functionalized with glucose oxidase and a mediator to allow selective detection of glucose in milk (Figure 2E).

With this wearable sensor-embedded platform, users can perform a single point measurement by connecting the sensors to a portable potentiostat when the pad is removed from the body for an electrochemical analysis (pad can be discarded afterwards). Alternatively, a flexible potentiostat (not discussed in this work) can be connected to the sensors on the lactation pad for continuous on-body analysis and wireless data transmission to the user's smartphone. In our previous work, we detailed the development of low-cost, open-source potentiostats.^[84,85] This article does not introduce new potentiostat circuit designs or include measurements using these detectors. To realize continuous monitoring, the milk sampling channel should be actively refreshed as new milk is leaked. To achieve this, we connected the milk-sampling microfluidic channel to the middle absorbent layer in the lactation pad (Figure 2C). Because of the water-absorbent silica gel in the middle layer, unpowered microfluidic pump and capillary force pulls the breast milk continuously, and fresh milk passes over the sensing allowing for frequent on-body analysis.

2.2. Optimization of Engraving Conditions for Electrode Fabrication

The electrochemical sensors in our wearable device are produced via laser engraving on polyimide polymeric sheets (PI, thickness of 125 μm) using a CO₂ laser beam with a wavelength of 9.3 μm. Laser engraving is a scalable, reproducible, and single-step process that forms high-quality graphitic structure without further physical or chemical processing.^[86] LIGs have a porous structure with high surface area, excellent electrical conductivity, and outstanding mechanical stability and flexibility, maintaining their electrochemical performance after several bending cycles.^[87] LIGs have been explored for the development of low-cost sensors in different applications including medical diagnosis,^[88–90] nutritional monitoring,^[85,91] and environmental applications.^[92] The structure electrochemical and mechanical properties of produced LIGs are significantly dependent on the delivered laser energy per unit area (laser fluence), which can be controlled through the engraving parameters, as in Equation (1).

$$\text{Laser fluence} = \frac{\text{Laser power}}{\text{Scan speed} \times \text{Beam diameter}} \quad (1)$$

To select and obtain the optimal parameters for engraving, we optimized the laser power and beam diameter at a fixed speed of 20% of the maximum engraving speed of the machine. Laser power was adjusted directly in the laser control software, and beam diameter was manipulated indirectly by changing the working distance between the laser focal point and the PI sheet surface (named defocusing distance). When the laser beam exits the lens, it forms a cone shape and converges until it reaches the

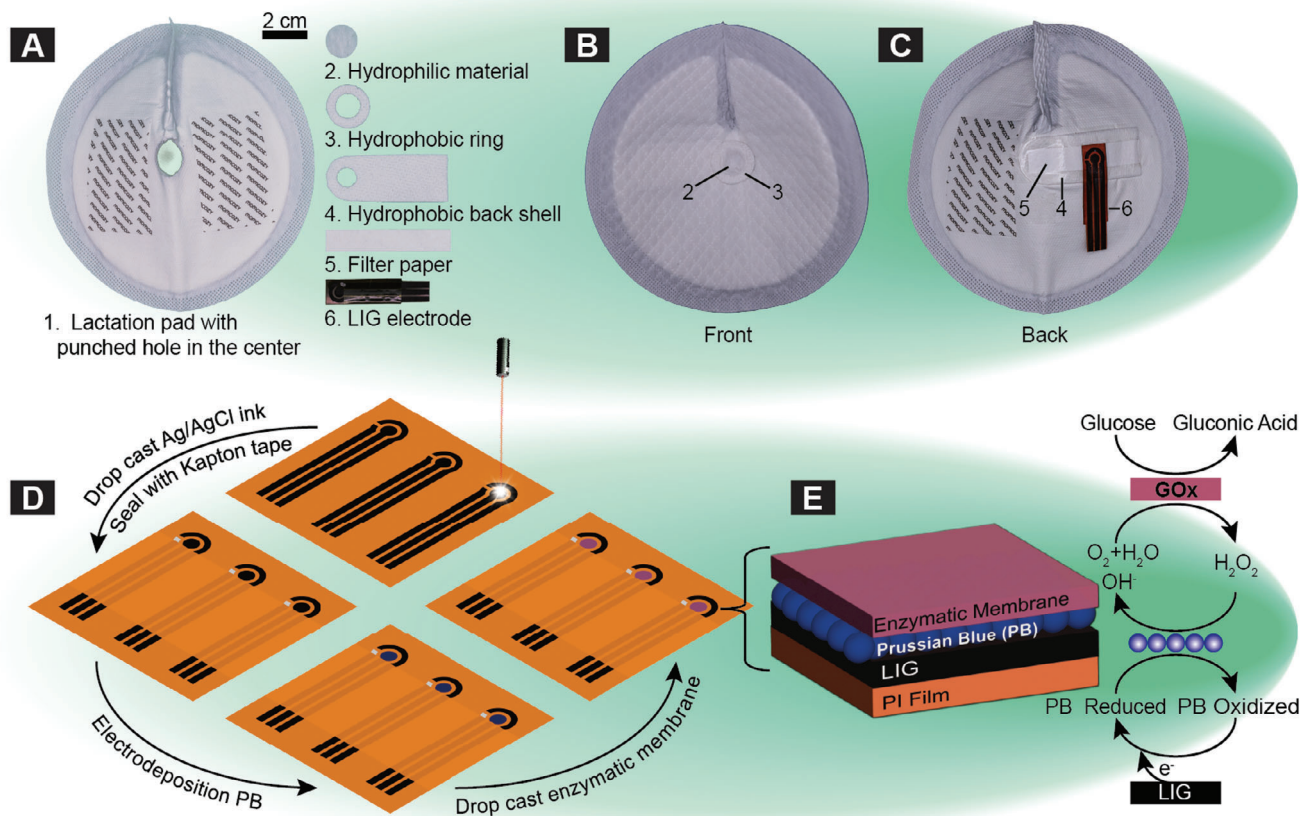


Figure 2. Fabrication of wearable sensor-embedded lactation pad. A) Photos of components used in the device fabrication. B,C) Photo of front and back of the smart lactation pad. D) The process for fabrication of laser-engraved electrodes and surface functionalization. PB stands for Prussian blue. E) The sensing mechanism for the detection of glucose using the enzyme-modified electrodes.

smallest spot size at the focal point. Therefore, increasing the distance between the laser focal point and the PI surface causes the laser beam to diverge before reaching the material, increasing the beam diameter.

Here, we selected the engraving parameters by comparing the electrical conductivity of the laser-induced graphene produced at power values between 1 and 19 % of the maximum power of our laser engraver (30 W) while changing the defocusing distance from 0.1 to 0.35 inch. Figure S1A shows a photo of the obtained LIG and the corresponding sheet resistance. It is noticeable that the PI film burns at a low defocusing distance even at low power values (7%), and by increasing the offset, the PI can tolerate more power and produce more conductive LIG film. While a larger beam diameter may decrease the laser's impact, potentially affecting the quality and conductivity of LIG, it enables overlapping of adjacent engraved spots and increases the number of engraving cycles per unit area. Consequently, it can still produce high quality graphene structures with good electrical conductivity, as shown in Figure S1B. For further work, we selected the power of 13%, a defocusing distance of 0.30 inch which produces mechanically stable LIG with low sheet resistance ($7.2 \Omega/\text{sq}$). The mechanical stability of the produced LIG was evaluated by measuring sheet resistivity after exposing the material to repeated bending cycles (150 degrees). As detailed in Figure S2 (Support-

ing Information), the electrodes demonstrated consistent sheet resistivity even after 50 bending cycles, confirming the mechanical robustness of the LIG and its suitability for integration into wearable devices.

The surface structure and morphology of LIG was evaluated via scanning electron microscopy (SEM). Figure 3A,C shows the top and cross-sectional view SEM images of the LIG, confirming the formation of a 3D porous foam-like carbon structure on the PI film with a thickness of about 50 μm . The obtained LIG structure provides a high active surface area and dense edge-plane sites providing electrodes with fast heterogeneous electron transfer rates and enhanced electrochemical sensitivity.

2.3. Development of the Glucose Biosensor

The optimized engraving conditions were followed to produce a three-electrode electrochemical system consisting of reference, counter, and working electrodes. The working electrode area has a diameter of 4 mm. Following engraving, the electrodes were washed with deionized water and dried in an oven at 60°C for 30 min. Silver/silver chloride ink was drop-cast onto the reference area (and cured at 60°C for 30 min) to establish a stable and consistent reference potential. Figure 4A shows the cyclic

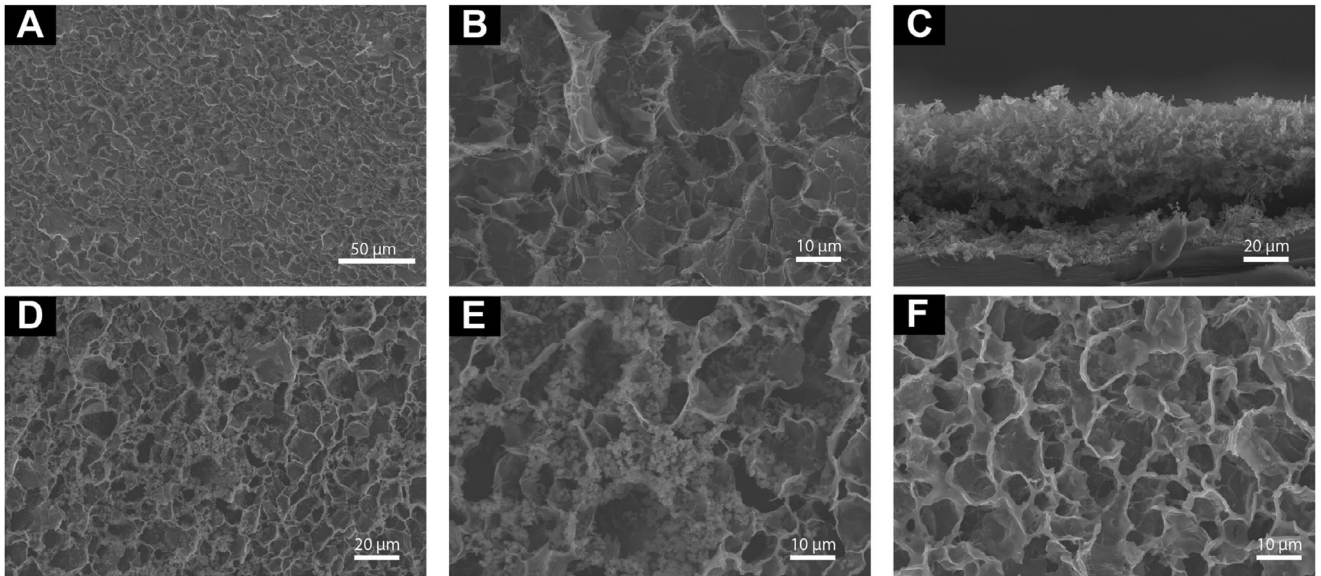


Figure 3. Scanning electron microscope (SEM) images of LIGs. A,B) Top view of bare LIG. C) Cross-section of bare LIG. D,E) Top view of LIG modified with Prussian Blue (PB). F) Top view of LIG modified with PB and glucose oxidase (GOx).

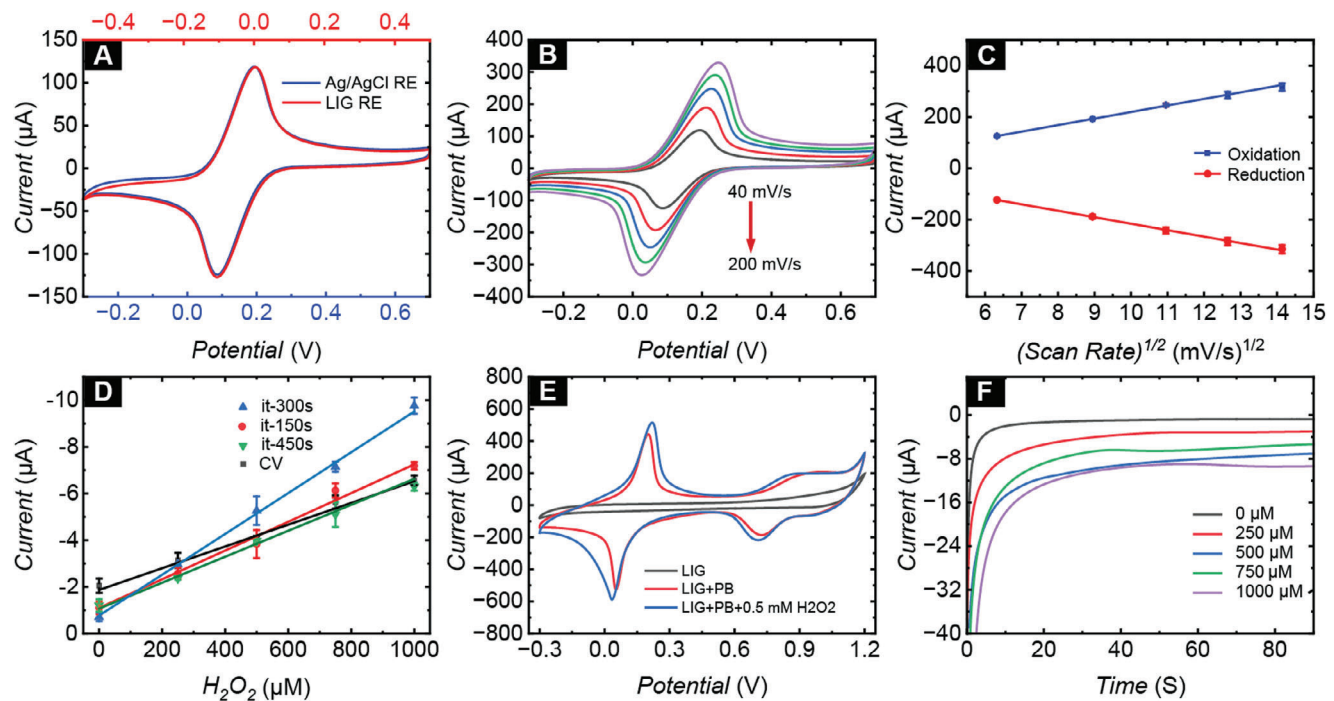


Figure 4. Electrochemical characterization of laser-induced graphene electrodes, showing outstanding electrochemical performance of these low-cost electrodes. A) Cyclic voltammograms (CV) for the LIG-based three electrode cell at scan rate of 40 mV s^{-1} in $2.0 \text{ mM} [\text{Fe}(\text{CN})_6]^{3-/4-}$ in 0.1 M KCl supporting electrolyte. The red trace uses a laser engraved carbon electrode as reference, while the blue trace employs the laser engraved carbon electrode covered with a Ag/AgCl ink, as reference electrodes. (B) CV of electrode at scan rates from 40 to 200 mV s^{-1} in $2.0 \text{ mM} [\text{Fe}(\text{CN})_6]^{3-/4-}$ in 0.1 M KCl supporting electrolyte. C) Oxidation and reduction current peaks versus $(\text{scan rate})^{1/2}$ (measured from corresponding CVs in B), showing a diffusion controlled redox process at the electrode. D) Calibration curves of LIG electrodes modified with PB in H_2O_2 . Electrical current was sampled at 90 s while electrical potential was held at 0 V . E) CV for bare LIG electrode and PB-modified LIG electrodes in PBS, and in PBS spiked with $500 \mu \text{M} \text{H}_2\text{O}_2$ at a scan rate of 50 mV s^{-1} . F) Amperometric signal curves (measured at 0 V) for PB-modified LIG electrodes at different concentrations of H_2O_2 . Standard deviation (SD) represents measurements with three different electrodes.

voltammograms (CV) for the LIG-based three electrode cell at scan rate of 40 mV s⁻¹ in 2.0 mM [Fe(CN)₆]^{3-/4-} in 0.1 M KCl supporting electrolyte. The blue and red trace show the CV measured before and after modification of the reference electrode with the Ag/AgCl, confirming the active electrochemical surface area is retained, while the reference potential has shifted by 200 mVs. Scan rate was altered in the CVs from 40 to 200 mV s⁻¹ (Figure 4B), and the linear increase of oxidation and reduction peak currents with the square root of the scan rates (Figure 4C) confirmed a diffusion controlled redox process at the surface of the LIG working electrode. The Randles–Sevcik equation (Equation 2) was used to analyze current peaks and calculating the active surface area of the developed electrodes.

$$i_p = 0.4463nFAC\sqrt{\frac{nFvD}{RT}} \quad (2)$$

In Equation (2), i_p is the current peak in amperes, n is the number of electrons transferred in the electrochemical event, F is Faraday constant in C/mol, A is the electrode area in mm², D is the diffusion coefficient in cm²/s, C is the electrolyte concentration in mol/cm³, v is the scan rate in V/s, R is gas constant in J/(K mol), and T is temperature in K. The active surface area of the LIG-based electrodes reached up to 58.17 ± 3.9 mm² ($n = 3$), demonstrating an enhancement in the surface area by approximately 4.63 ± 0.31 ($n = 3$) times greater than the geometric area (12.57 mm²).

We deposited prussian blue (PB) (Fe₄[Fe(CN)₆]₃), on the working electrode as the mediator in the enzymatic reaction. Mediators are commonly used in electrochemical enzymatic sensors to lower the measurement potential and subsequently decrease the chance of non-specific signal from electrochemically active interfering molecules.^[45,93–95] Mediators react with the hydrogen peroxide that is produced in the enzymatic reaction (Figure 2E), and are then detected at the working electrode at a lower electrical potential. The LIG working electrode was electrochemically functionalized with Prussian Blue (PB) (Fe₄[Fe(CN)₆]₃). PB can be electrodeposited onto the working electrode using various electrochemical techniques, including amperometry and cyclic voltammetry.^[96–98] The electrodeposited PB's crystallinity, particle size, and activity in hydrogen peroxide H₂O₂ reduction significantly depend on the electrodeposition parameters and electrode electrochemical properties. In this work, a deposition solution was prepared using 5 mM FeCl₃, 5 mM K₃Fe[CN]₆, 0.1 M KCl, and 0.1 M HCl in deionized water. PB was deposited at four different electrochemical conditions and we selected the most appropriate conditions by comparing electrode sensitivity toward H₂O₂ in a concentration range between 0 and 1000 μM in phosphate-buffered saline (PBS). We compared the deposition using an amperometric technique at a fixed potential of 0.4 V versus external Ag/AgCl reference electrode for a time duration of 150, 300, and 450 s. Also, we compared that with PB-modified electrodes functionalized using CV at a potential window between -0.3 and 0.7 V at a scan rate of 100 mV s⁻¹ for 10 cycles. After that, the PB-modified LIG electrodes were cleaned using cyclic voltammetry (window from -0.3 to 0.7 V) using a solution of 0.1 M HCl and 0.1 M KCl at a scan rate of 50 mV s⁻¹ until the voltammograms displayed consistent and reproducible shapes and current values. Then the electrodes were left to dry overnight at room tempera-

ture. Figure 4D shows the comparison of the four PB deposition conditions in detecting H₂O₂ in PBS solution at an applied potential of 0 V. We notice that all the parameters demonstrated linear amperometric response toward H₂O₂ in a wide range of concentrations, up to 1000 μM, with differences in the slopes of the obtained calibration curves. Utilizing amperometric deposition for 300 s demonstrated the highest sensitive behavior with a slope of 0.009 μA/μM, therefore we used these parameters for all the further experiments.

SEM images (Figure 3D,E) of the PB-modified LIG electrodes demonstrated the uniformly distributed nanoparticle clusters on the electrode surface. The clusters are localized primarily on the edge sites enveloping the inner regions of the porous structure. Figure 4E depicts the cyclic voltammograms of bare LIG and PB-modified LIG electrodes in PBS solution. We observed no peaks appearing in the bare electrodes, while we got four distinctive peaks of the PB-modified LIG electrodes representing the characteristic two redox processes of PB films. The first process at E_{1/2} = 0.18 V indicates the PB/Prussian white (PW) couple while the one at E_{1/2} = 0.85 V represents Berlin green (BG)+PB pair.^[99] CV for PB-modified LIG in 500 μM of H₂O₂ demonstrated higher redox current at 0 and slightly negative potentials confirming the catalytic behavior of the PB in H₂O₂ detection electrodes.

We used the Raman spectroscopy technique to characterize the structural fingerprints of LIG and LIG+PB. The Raman spectrum of LIG showed the main peaks of the graphene structure, as shown in Figure 5A. The peak at ≈1580 cm⁻¹ (G peak) indicates the sp² carbon atoms vibration in the graphene lattice, while the D peak (at ≈1350 cm⁻¹) represents the structural disorders and defects present in the sigma bonds in the graphene structure.^[91,100] The 2D peak at ≈2692 cm⁻¹ represents the two-phonon scattering process in the arrangement of graphene atoms. The LIG's Raman spectrum showed an I_{2D}/I_G ratio of around 0.42. This value suggests the presence of multiple graphene layers, as reported in previous research.^[101] After the electrochemical deposition of Prussian Blue, Raman spectroscopy demonstrated the appearance of a sharp peak at 2159 cm⁻¹ because of the symmetric stretching vibration of the triple bond in –C≡N in Fe^{II}–C≡N–Fe^{III} structure. The weaker peak at 2097 cm⁻¹ is ascribed to the asymmetric stretching vibration of the Fe^{II}–C≡N–Fe^{III}.^[102–104] Energy-dispersive spectroscopy (EDS) was used to analyze LIG before and after depositing PB. For bare LIG, Figure 5C demonstrates an intense peak at the carbon-characteristic binding energy indicating successful carbonization of the PI polymer through laser engraving. Notably, no detectable peaks were observed for nitrogen or oxygen, elements inherently present in the PI. This absence supports the effectiveness of the carbonization process. The EDS spectrum of the LIG+PB surface reveals additional peaks corresponding to iron, potassium, and carbon. Those items are the expected in the two forms of Prussian blue; Fe₄K₄[Fe(CN)₆]₃ and Fe₄[Fe(CN)₆]₃. Also, the presence of chloride (Cl) observed in the EDX spectrum likely originates from residual KCl and HCl used during the PB electrodeposition process. To further investigate the elemental composition and chemical bonding states within the fabricated pristine and PB-modified LIG surfaces, we employed X-ray photoelectron spectroscopy (XPS) analysis. Figure 5D,E demonstrate the high-resolution peak spectra of

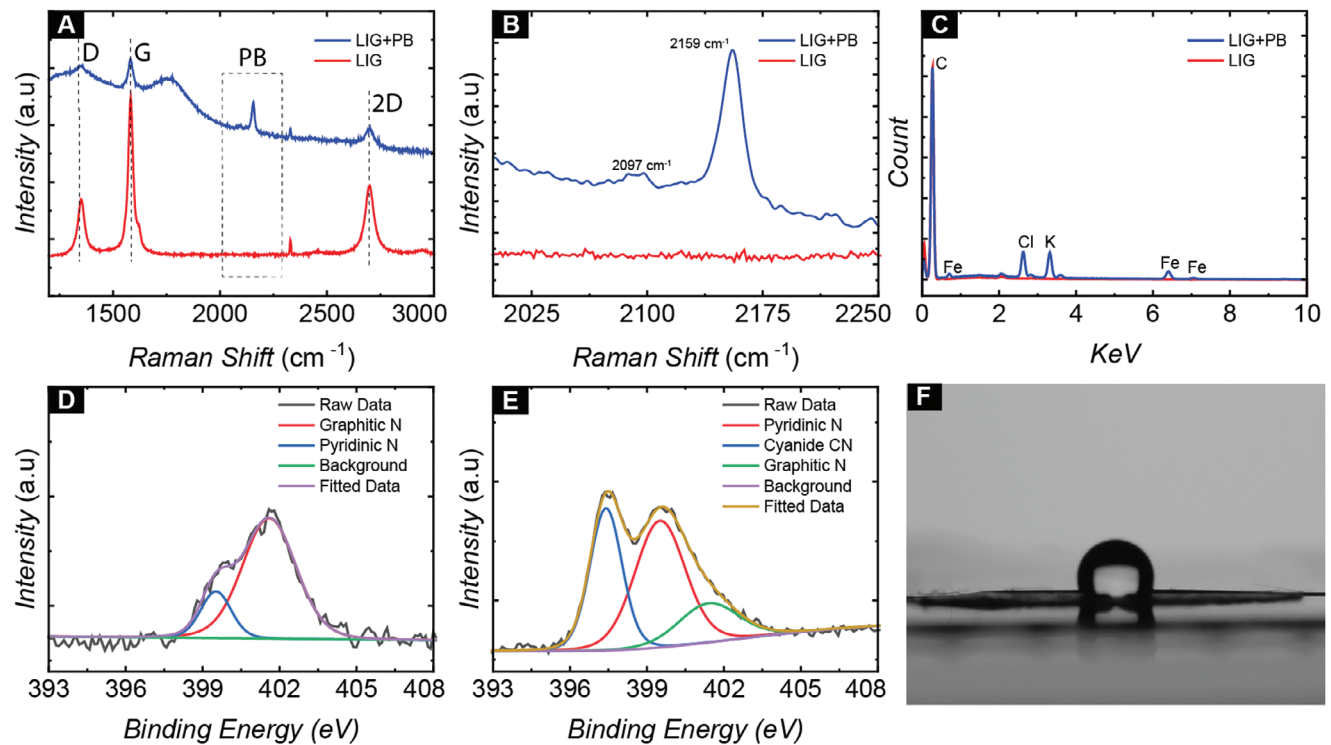


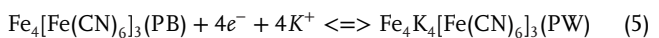
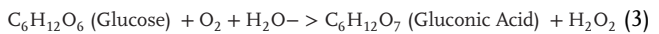
Figure 5. Material characterization of bare and modified LIG. A) is Raman spectra of LIG and LIG+PB. B) PB-related peak region in Raman Spectra of pristine and PB-modified LIG electrodes. C) EDS spectra of pristine and PB-modified LIG electrodes. Panels (D) and (E) are N 1s high-resolution XPS peaks for pristine and PB-modified LIG electrodes, respectively. F) is the water contact angle of the LIG modified with PB and GOx membrane.

N 1s peak for the LIG, and LIG+PB, respectively. Analysis of LIG's peak results in two peaks at 399.5 and at 401.6 eV corresponding to the pyridinic and graphitic nitrogen, respectively. After the modification with PB, another peak emerged at 397.4 eV which likely corresponds to the cyanide N (C≡N) that exists in PB.^[105–107] Survey and high-resolution C 1s and N 1s spectra did not show any detectable difference between pristine and PB-modified LIG (Figure S3, Supporting Information).

After demonstrating that PB-modified LIGs respond effectively to H₂O₂, an enzymatic glucose sensing membrane was added on the electrode surface. Briefly, three solutions were prepared in the beginning as follows: 1% bovine serum albumin (BSA) in PBS, 0.5 % glutaraldehyde (GA) in deionized water, and 0.5 % Nafion in deionized water. After that, 4.0 mg Glucose Oxidase (GOx) was dissolved thoroughly in 100 μL of the BSA solution before adding 100 μL of the GA solution, and 35 μL of the Nafion solution. Then, 4.0 μL of the obtained solution was drop cast on the electrode surface and dried at ambient conditions for 24 h to form a homogeneous enzymatic membrane on the surface. The membrane formulation was used for cross-linking BSA and GOx with GA to attach the enzyme to the electrode surface and provide a protective layer for the enzyme that maintains enzyme activity and improves the sensor's performance and shelf life. Nafion has also been proven to enhance the sensitivity and selectivity of enzymatic sensors by eliminating interference and providing high diffusivity for glucose and oxygen.^[74,108–110]

The surface structure of the glucose enzymatic sensor (LIGs modified with PB and GOx) (Figure 3F) shows the formation of a uniformly thick layer coating the LIG structure and PB particles

on the electrode surface indicating the successful cross-linking of GA, GOx, and BSA on the electrode surface. Furthermore, water contact angle measurements were employed to characterize the surface wettability of the developed sensor electrodes. Bare and PB-modified LIG electrodes exhibited highly hydrophilic surfaces. Water droplets rapidly expanded and spread across electrode porous structures. However, deposition of the GOx membrane, the surface showed a significant increase in hydrophobicity with a contact angle of 102°, as shown in Figure 5F. This observation suggests the successful polymerization of BSA and GOx by GA molecules. The mechanism of work of the developed biosensor is illustrated in Figure 6A and Equations (3, 4, 5). At the interface between the biosensor and the solution, GOx catalyzes the oxidation of glucose in the presence of O₂ and H₂O, yielding gluconic acid and H₂O₂. On the electrode surface, at a zero or slightly negative potential, Prussian Blue (PB) is reduced to Prussian White (PW). Subsequently, PW reacts with H₂O₂, reducing it to OH⁻ while being oxidized to regenerate PB. PB is then reduced back to PW, completing a cycle of chemical reactions. The electrochemical cathodic current generated in this process corresponds to the produced H₂O₂, and sequentially the oxidized amount of glucose, allowing for the indirect quantification of glucose concentration in the sample.^[98,111–116]



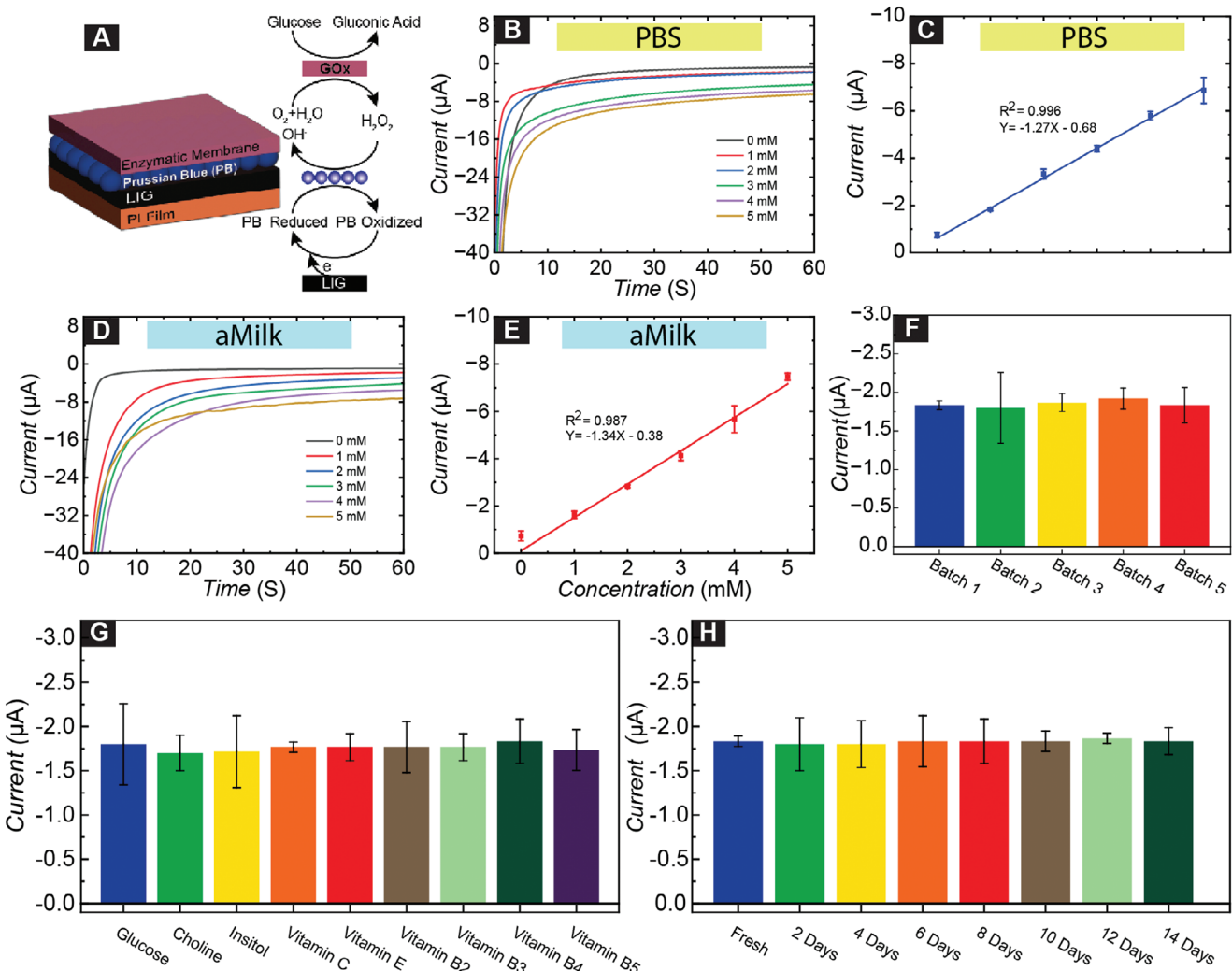


Figure 6. A) The mechanism of work of the developed Glucose biosensor. B) I-t amperometric responses for the glucose biosensor toward glucose in PBS solution. C) The calibration curve of the glucose sensor in PBS solution. D) I-t amperometric responses for the glucose biosensor toward glucose in aMilk solution. E) The calibration curve of the glucose sensor in aMilk solution. F) Batch-to-batch variability of the produced glucose biosensor. G) Selectivity of the glucose biosensor toward glucose in the presence of interfering milk components. H) Shelf life measurements of the biosensor after storage for different periods of time. I-t measurements were conducted at 0 V potential and SD represents three different measurements.

The i-t amperometry technique was used to detect glucose using the developed PB and GOx modified LIG, at a constant potential of 0 V. As depicted in Figure 6B, the amperometric i-t current responses of the fabricated biosensor were recorded at a glucose concentration range between 0 and 5.0 mM in PBS solution. The biosensor exhibited a concentration-dependent response, with a direct correlation between the measured current and increasing glucose concentration. The higher glucose concentrations resulted in a higher magnitude of the recorded current. The steady-state current at 60 seconds was selected to establish a calibration curve for the biosensor (Figure 6C). The sensor demonstrated a linear relationship between its electrochemical response and glucose in PBS within the studied range (0 to 5 mM) with a slope of $-1.27 \mu\text{A} \text{ mM}^{-1}$, an intercept of $-0.62 \mu\text{A}$, and R^2 of 0.996. The corresponding LOD of the calibration curve in PBS (calculated from $(\text{LOD} = 3.3 \text{ SD/slope})$) is about 0.15 mM. These performance characteristics are suitable to quantify the

glucose levels in human milk as a physiological glucose concentration of 1–4 mM is expected in human milk under normal, hypoglycemic, and hypoglycemic conditions. Table S1 (Supporting Information) compares the analytical performance of the developed device with other PB-based glucose biosensors designed for biofluids like blood serum, sweat, and interstitial fluid.

2.4. Selectivity and Shelf-life of the Glucose Biosensor

To verify and test the practical usability of this sensor in human breast milk, we evaluated its performance in artificial milk (aMilk), which mimics the molecular composition of human milk.^[117–119] The aMilk solution was prepared from 7.0 mM NaCl, 18.0 mM KCl, 13.0 mM CaCl₂, and 2.0 mM MgCl₂, 12.0 μM vitamin E, 2.0 μM vitamin B1, 2.1 μM vitamin B2, 2.8 μM vitamin B6, 20.0 μM Vitamin B3, 12.0 μM vitamin B5, 300.0 μM

inositol, 348.0 μ M Vitamin C. Figure 6D shows the obtained i-t amperometry response of the glucose sensor toward glucose levels between 0 to 5 mM in aMilk cocktail. The sensor demonstrated increasing in the current response while increasing the glucose concentrations, and the calibration curve. Figure 3E, shows a linear response in the range of 0–5 mM with a slope of –1.34, intercept of –0.38, confirming that the linearity and sensitivity of the developed biosensor is suitable for quantifying glucose levels in human milk samples.

Batch-to-batch variability in enzymatic sensors can significantly impact their reliability and accuracy. In this work, we fabricated five different batches of enzymatic sensors, fabricated on different days, deposited with different PB solutions, and enzymatic membranes. We compared their performance toward 1 mM glucose in PBS solution. We observed no significant difference in recorded currents between batches indicating consistency in manufacturing processes and performance (Figure 6F). To verify the accuracy of the glucose biosensor in detecting glucose within human milk, we assessed its selectivity by comparing its response to glucose against other milk components, including choline, inositol, and vitamins E, B2, B3, B4, and B5. The sensor's response to 1 mM glucose in PBS was measured and compared to its response when 1 mM glucose was combined with 1 mM of each interfering molecule, tested individually. Figure 6G shows that the sensor maintained a consistent response to the 1 mM glucose solution, even in the presence of these potential interferents, indicating minimal interference from the additional components. The selective performance of the developed glucose biosensor is attributed to the enzymatic membrane, which effectively prevents interference from substances from reaching the electrode surface. Furthermore, the used potential for measurements (0 V) is insufficient to oxidize or reduce other components present in the solutions. These factors collectively contribute to the biosensor's ability to selectively detect glucose in complex biological matrices including human milk.

Investigating the shelf life stability of biosensors is significantly important to consider in the development of biosensors, since the used enzyme could lose its functionality during storage, leading to false measurements. Here, we investigated the shelf-life of our sensor by keeping sensors stored in the fridge at 4 °C for time periods ranging from 0 to 14 days, before test them in 1 mM glucose in PBS solution. Sensors maintained their performance after 14 days of storage (Figure 6H), which can be attributed to the biocompatible environment that BSA, GA, and Nafion created protecting the enzyme and maintaining its functionality.

2.5. Sensor Integration in a Smart Lactation Pad

We integrated the glucose sensor in a lactation pad (commonly worn during the day by lactating mothers to absorb leaked milk) to enable a seamless milk sampling and analysis during the day, without adding extra burdens on the already busy parents. A lactation pad consists of three main layers: a thin porous membrane that contacts the skin, an absorbing material to capture milk leakage throughout the day, and a water-proof barrier that protects the clothing against leakage. We modified a commercial lactation pad with a hydrophobic ring that separates a central portion from the

rest of the absorbing material (Figure 2A,B). The inlet of a microfluidic channel made of filter paper was placed at this isolated central portion to capture some of the leaked milk and direct it to the sensing zone by capillary wicking. This paper-based microfluidic channel and the sensors are placed on the back of the pad on the water-proof layer to prevent sample contamination by the absorbing material in the pad. The outlet of the microfluidic channel is connected back to the absorbing material through an incision in the waterproof layer. This connection induces negative fluid pressure that milk to wick along the channel and allows the sensor to access fresh milk over time (Figure 7A). Details of device fabrication are listed in the experimental section. In brief, we punched a hole in the bra pad, sandwiched a LIG electrode between a skin-facing hydrophobic circle (cut from a hydrophobic soft textile, safe for skin contact) and the filter paper, and secured the layers together using a biocompatible clear tape. In addition to keeping the layers secured, the tape also minimizes evaporation as the milk travels in the fluidic channel.

In this integrated lactation pad, the microfluidic channel has a dead volume of 400 μ L, and can be filled in 60 s, shown with an aqueous blue dye in Figure 7B,C. As indicated by the arrow, the blue dye saturated the paper channel and appeared on the absorbing material, then continued to spread through the absorbing material for 60 s. We then validated fluid flow and stable contact with the LIG electrode using CV. We added 2.0 mM $[\text{Fe}(\text{CN})_6]^{3-/4-}$ (in 100 mM KCl as supporting electrolyte) to the fluid inlet of the lactation pad and measured CVs at 0, 30, 60, and 90 s after fluid addition. As shown in Figure 7D, a stable CV can be achieved 60 s after adding the fluid. We then confirmed that LIG-based glucose sensors can accurately measure glucose in milk when they are integrated in a lactation pad. Since milk composition changes as the infant develops, we tested our sensing platform using breast milk samples collected at one, six, and twelve months postpartum to evaluate its ability to accurately measure glucose levels. This allowed us to assess the sensor's performance across varying milk compositions and potential interfering substances.

We employed a direct addition method, measuring glucose concentration directly in the milk samples using the calibration curve generated with aMilk samples (Figure 6E). Subsequently, the milk samples were spiked with known amounts of glucose (1.0 and 2.0 mM) to evaluate the accuracy of measurements. Figure 7E–G shows the i-t amperometric curves of the three samples at the three different glucose concentrations. Accuracy was calculated based on the expected value after spiking (original glucose level in milk plus the spiked concentration). Table 2 shows the results. The average spike recoveries ranged between 96.8 and 104.1% and the standard deviation (SD) between 3.7% and 8.3%. As shown in Figure 7H, the calibration curves for all three samples (1, 6, and 12 months) exhibit comparable slopes (–1.37, –1.37, and –1.25 $\mu\text{A mM}^{-1}$, respectively). This consistency across varying lactation stages, alongside the similarity to the reference milk calibration curve ($-1.34 \mu\text{A mM}^{-1}$), confirms that the sensor effectively measures glucose despite the presence of other interfering components that might be present in breast milk at different stages of lactation.

To confirm the channel refresh time (removing the old milk sample and replacing it with new milk), we initially performed studies with the same milk but spiked with glucose with different concentrations. We then first added 200 μL of breast milk samples

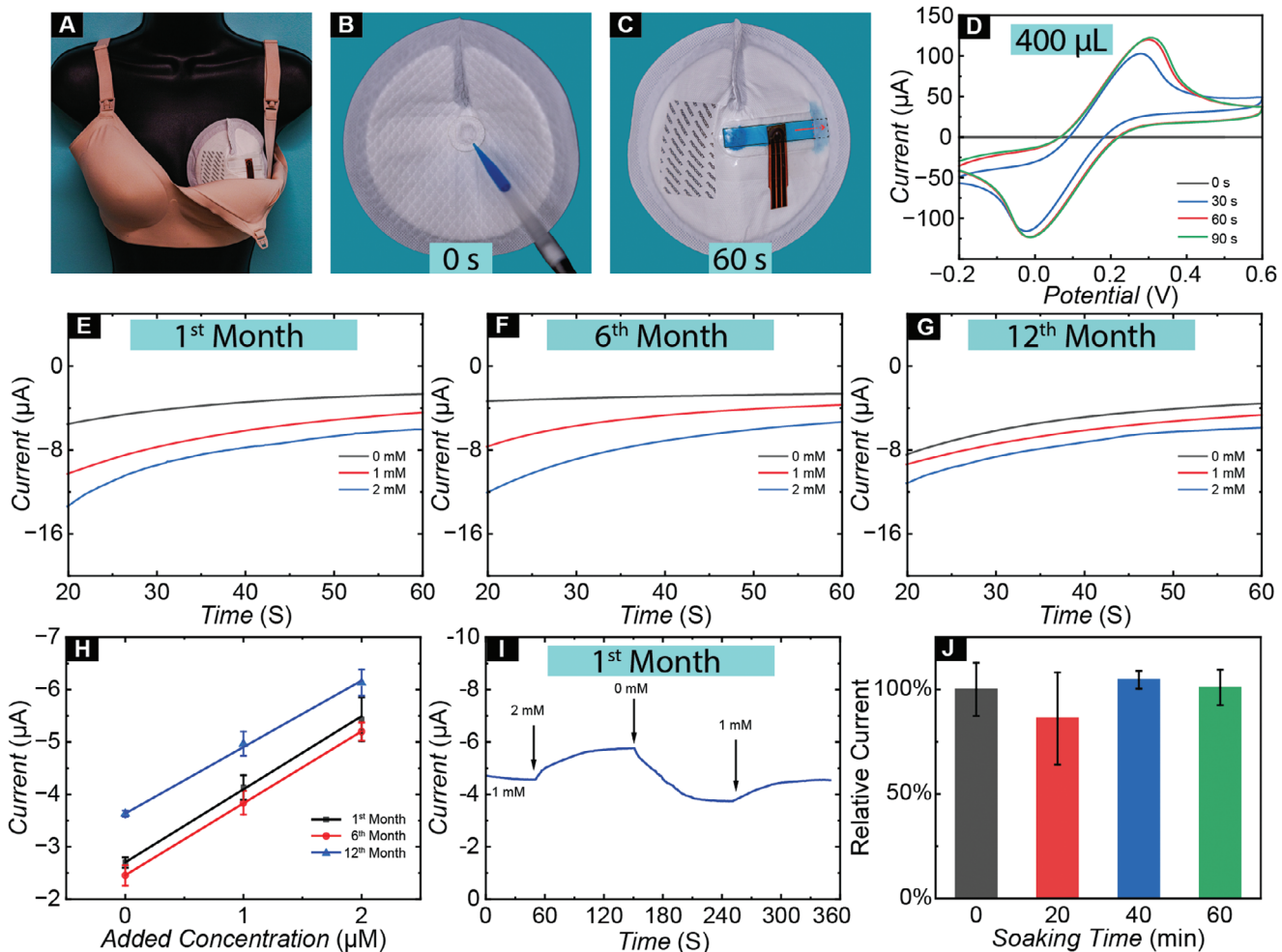


Figure 7. A) An image of the wearable sensor-embedded nursing bra pad. B,C) Flow test by adding 400 μ L breast milk with blue dye into our device at beginning and after 60 seconds. The black border indicates the paper strip added on the back of lactation pad and the red arrow indicates flow direction while dash line shows the part of paper strip buried in the lactation pad and connected to the absorbing material. D) Cyclic voltammograms of our device added with 400 μ L electrolytic solution of 2.0 mM $[\text{Fe}(\text{CN})_6]^{3-/4-}$ in 100 mM KCl at 0, 30, 60, and 90 s. E–G) I-t amperometric traces of actual human milk nonspiked and spiked with 1 mM and 2 mM glucose. (E) is milk taken in the first lactating month, where (F) and (G) are taken in the 6th and 12th month respectively. H) Calibration curves obtained between the added glucose concentrations and the corresponding currents for the three milk samples. I) I-t current changes while injecting human milk with different spiked glucose concentrations. J) Biosensor response of relative current toward actual human milk after 0, 20, 40, and 60 min of soaking. I-t measurements were conducted at 0 V potential and SD represents three different measurements.

Table 2. Detection accuracy of the Smart Nursing Bra Pad for glucose quantification in human milk samples taken at the first, sixth, and twelfth month of lactation ($n=3$).

Milk Sample	Added Concentration (mM)	Measured Concentration \pm SD (mM)	Recovery Percentage \pm RSD(%)
1st Month	0	1.72 \pm 0.07	—
	1 mM	2.79 \pm 0.17	102.4 \pm 6.3
	2 mM	3.76 \pm 0.3	100.9 \pm 8.3
6th Month	0	1.47 \pm 0.15	—
	1 mM	2.57 \pm 0.17	104.1 \pm 6.8
	2 mM	3.58 \pm 0.13	103.2 \pm 3.7
12th Month	0	2.42 \pm 0.04	—
	1 mM	3.41 \pm 0.17	99.8 \pm 5.7
	2 mM	4.27 \pm 0.19	96.8 \pm 4.2

spiked with 1 mM glucose in the channel and after 60 seconds, began the amperometry measurement. With continuous amperometry recording, we added 100 μ L of breast milk samples spiked with additional 2 mM glucose or none to the inlet. The current signal changed after adding new samples and reached stable states after 120 secs, confirming that the smart lactation pad can monitor dynamics of glucose in milk with a temporal resolution of 2 mins. In Figure 7I, we show the amperometric response of LIG-based glucose sensors in the smart lactation pad, as milk solutions with different glucose concentrations are added to the inlet (labeled with arrows), confirming that the signal can increase and decrease as glucose levels change in milk, and confirm the device's ability for continuous monitoring throughout the day. For these experiments, a milk collected at one month postpartum was used which has the highest fat content and viscosity among our three samples.

To identify any potential effect of continued exposure to milk on the sensor performance, the sensor was submerged in breast milk for varying duration (0, 20, 40, and 60 min) before glucose measurements were carried out. The sensors maintained a consistent response even after 1 h of being soaking in milk (Figure 7J). This indicates the sensor's practical suitability for long-time monitoring and on-body measurements.

3. Conclusion

Women's health has often been underrepresented in research, leading to significant knowledge gaps. This study introduces the first wearable sensor designed to sample and analyze breast milk, addressing a critical unmet need in the biochemical analysis of human milk. Although our platform technology enables on-body milk capture and transport to a sensing zone for analysis of a broad range of biomarkers, glucose was chosen as the initial biomarker. Glucose plays a critical role in the physical and neurological development of infants and children. Just as in adults, maintaining proper glucose levels is essential to avoid hyperglycemia and hypoglycemia, both of which can lead to long-term neurological impairments, seizures, and growth abnormalities. The few services available for evaluating breast milk composition require parents to collect and ship large volumes of milk using expensive kits (often costing over \$100). The samples are then analyzed in a lab, with results typically taking several weeks to be returned. Wearable devices have the potential to address this gap, but they have only been designed to sample and monitor biofluids such as sweat, tears, and wound exudate. Human milk—a vital source of information on maternal health and infant nutrition—has largely been overlooked. Research on at-home or point-of-care breast milk analysis also remains sparse. This work introduces a novel combination of materials to create a wearable sensor integrated into a lactation pad—a familiar accessory for lactating mothers traditionally used to absorb leaked milk. For the first time, this study embeds sensors and microfluidic channels within a lactation pad, transforming it into a multifunctional device capable of continuous biochemical analysis of breast milk as it leaks throughout the day. This groundbreaking innovation redefines the functionality of a common postpartum accessory, bridging convenience and advanced health monitoring. This innovation also pioneers the development of accessible and afford-

able tools for breast milk analysis, addressing the scarcity of cost-effective sensors for the analysis of human milk.

We developed an electrochemical sensing platform using laser-induced graphene (LIG) electrodes, fabricated via laser engraving on a thin polyimide film. This process enables scalable, mask-free, and cost-effective sensor production. The enzymatic membrane, composed of glucose oxidase, glutaraldehyde, BSA, and Nafion, further protects the enzyme and extends the sensor's functionality, allowing it to detect glucose concentrations within the physiologically relevant range for human milk. The sensor's sensitivity, selectivity, and accuracy were evaluated in buffer, synthetic milk, and undiluted human milk samples collected from different donors at various lactation stages (1st, 6th, and 12th months). The wearable glucose sensing platform demonstrated high accuracy, measuring glucose concentrations in the range of 1 to 5 mM, which fully covers the physiological range in human milk, with a performance of 96.8% to 104.1% accuracy across different lactation stages. The sensor also exhibited stability when soaked in human milk for over an hour, with the enzymatic membrane effectively protecting both the enzyme and the electrode from biofouling. Shelf-life stability was confirmed for up to two weeks of storage. Additionally, the wearable lactation pad successfully measured dynamic glucose concentration changes, utilizing its absorbent material to refresh the microfluidic channels. This achievement marks the first continuous measurement of any biomarker in human milk via a wearable device. It also introduces the first glucose and electrochemical sensor specifically designed for use in human milk, laying the foundation for a paradigm shift in maternal and infant healthcare by enabling proactive monitoring and timely interventions.

This innovative smart lactation pad empowers mothers to actively monitor their health and their baby's nutrition in real time, and make clinical decisions in consultation with their medical team. Beyond its applications for parents and infant health, the platform facilitates continuous data collection, offering deeper insights into dynamic changes in milk composition throughout the lactation period, particularly in relation to carbohydrate content. Future work will expand this platform to detect additional metabolites, disease markers, nutritional factors, and drug levels in breast milk.

4. Experimental Section

Milk Samples: All experiments involving human samples were approved by the Institutional Review Board of the University of Southern California (HS-23-00356), with all procedures following relevant guidelines and regulations. Human breast milk samples were obtained from Mothers' Milk, a third-party milk bank registered with the FDA, accredited by the Human Milk Banking Association of North America (HMBANA), and licensed as a tissue bank in California. In compliance with OHRP regulation 45 CFR 46.104, informed consent was waived to maintain donor anonymity, as the samples were deidentified and contained no information linking them to the donors.

Materials and Reagents: Adhesive Back, Electrical-Grade, Kapton® Polyimide Film was purchased from McMaster-Carr, USA. We utilized potassium ferricyanide, potassium Hexa-Cyanoferate (II) Trihydrate, D-glucose, hydrogen peroxide solution, Nafion® perflourinated resin solution, glucose oxidase from *Aspergillus Niger*, glutaraldehyde solution, and bovine serum albumin from Sigma Aldrich. Additionally, ferric chloride hexahydrate and phosphate-buffered saline (PBS

1x) without calcium and magnesium ($\text{pH } 7.4 \pm 0.1$) were obtained from VWR Chemicals and Corning Incorporated, respectively. Deionized water (Resistivity of $(18.2 \text{ M}\Omega \cdot \text{cm})$) was used to prepare aqueous solutions.

Electrode Fabrication: The Kapton polyimide film was sequentially washed with acetone, 70% isopropyl alcohol, and deionized (DI) water before dried in an oven at 60°C for 30 minutes. The cleaned film was then loaded into a laser engraver machine (VLS2.30, Universal Laser Systems Inc.) equipped with a laser source with 30 W power and $9.3 \mu\text{m}$ wavelength. The engraving was conducted at raster mode. Next, Kapton tape was applied to define the working electrode area. Then, Ag ink was applied for the reference electrode, and dried at 60°C for another 30 minutes. PB was deposited on the electrode surface using i-t amperometric technique at fixed potential of 0.4 V for 300 s using a solution of 5 mM FeCl_3 , 5 mM $\text{K}_3\text{Fe}[\text{CN}]_6$, 0.1 M KCl and 0.1 M HCl in deionized water and external Ag/AgCl reference electrode (glass frit, 1 M KCl reference solution). The electrodes were then electrochemically cleaned using cyclic voltammetry in a solution of 0.1 M HCl and 0.1 M KCl. The scan window ranged from -0.3 V to 0.7 V at a scan rate of 50 mV s^{-1} . This cleaning process was continued until stable peaks were achieved. Afterward, the electrodes were left to dry overnight at room temperature. The composition of the glucose sensing membrane was selected based on prior work on glucose sensing in other biofluids.^[93,120,121] To develop the glucose sensor, three solutions were first prepared: 1% bovine serum albumin (BSA) in PBS, 0.5% glutaraldehyde (GA) in DI water, and 0.5% Nafion in DI water. Then, 4.0 mg glucose oxidase (GOx) was thoroughly dissolved in $100 \mu\text{L}$ of the BSA solution. Subsequently, $100 \mu\text{L}$ of the GA solution and $35 \mu\text{L}$ of the Nafion solution were sequentially added to the BSA-GOx mixture. $4.0 \mu\text{L}$ of the resulting solution was drop-cast onto the electrode surface and allowed to dry at ambient conditions for 24 h.

Fabrication of the Smart Lactation Pad: First, a steel hollow punch (diameter of 1.23 cm) was used to create a hole in the center of a commercial (Momcozy, ultra thin, 0.16 cm) disposable lactation pad and the removed material (2 in Figure 2A) was saved for the next steps. The hydrophobic fabric material (ProSoft FoodSAFE REPREVE Waterproof PUL Fabric, AKAS Tex LLC) was punched to a ring shape (3 in Figure 2A) with inner diameter of 1.11 cm and outer diameter of 1.91 cm. It was then attached to the front side of the lactation pad (1 in Figure 2A) right above the hole by permanent double-sided tape (Scotch, 3M). There was another back shell part (4 in Figure 2A) fabricated from same hydrophobic material with same outer diameter but a smaller inner diameter of 0.95 cm. It was then attached to the back of the nursing pad to build the hydrophobic barrier to separate the absorbing material from the microfluidic channel. After building the hydrophobic barrier, the hydrophilic fabric (2 in Figure 2A) was peeled from the portion removed from the pad, and attached back to the middle hole of lactation pad surrounded by the hydrophobic material. The paper microfluidic channel was laser cut (5 in Figure 2A, Whatman qualitative filter paper, Grade 1) and the laser induced graphene electrode (6 in Figure 2A) were attached on the back of the lactation pad. The paper-based microfluidic channel was connected to the absorbing material in the lactation pad through an incision made in the hydrophobic cover on the back of the pad (as shown in Figure 1C). As a final step, transparent tape was utilized to cover both paper and electrodes from the back of the lactation pad to avoid leaking of breast milk from the cellulose paper, to slow down the milk evaporation, and to make better contact between the paper and the LIG electrodes.

Statistical Analysis: Data presented in this work represent the mean value \pm standard deviation, typically calculated from three independent measurements (unless otherwise specified). Mean, standard deviation, and linear regression calculations were performed using Microsoft Excel.

Supporting Information

Supporting Information is available from the Wiley Online Library or from the author.

Acknowledgements

A.A. and H.M. contributed equally to this work. This work was supported by the 3M Nontenured Faculty Award, Seed funding from the Women in Science and Engineering, Center for Sustainable Solutions, and Collaborative Research funding all from the University of Southern California (USC), as well as the NIH Director's New Innovator Award (DP2GM150018). A. A., H. M., F. A., M. B., A. S., and S. K. N. thank the USC Viterbi School of Engineering for Graduate Fellowship. All authors thank the Core Center of Excellence in Nano Imaging at the University of Southern California and Tom Czyszczon-Burton for their suggestion in X-ray photoelectron spectroscopy characterization. All authors would like to extend their gratitude to Cu Ho and Nhat Nguyen and all of the team at Mother's Milk for their collaboration in this endeavor and commitment to improving the health of mothers and children everywhere.

Conflict of Interest

The authors declare no conflict of interest.

Data Availability Statement

The data that support the findings of this study are available from the corresponding author upon reasonable request.

Keywords

breast milk, glucose biosensor, gestational diabetes, infant wellness, laser induced graphene, smart lactation pad, wearable devices

Received: October 31, 2024

Revised: January 20, 2025

Published online: February 16, 2025

- [1] K. M. Meyer-Abich, *Public Health Nutrition* **2005**, *8*, 738.
- [2] R. Kumar, S. Kumar, S. S. Kanwar, in *Biomedical Perspectives of Herbal Honey*, Springer, **2024**, pp. 1–17.
- [3] A. Ajibola, J. P. Chamunorwa, K. H. Erlwanger, *Nutrition & Metabolism* **2012**, *9*, 1.
- [4] J. R. Reeve, L. A. Hoagland, J. J. Villalba, P. M. Carr, A. Atucha, C. Cambardella, D. R. Davis, K. Delate, *Adv. Agron.* **2016**, *137*, 319.
- [5] M.-S. Lee, Y. C. Huang, H. H. Su, M. Z. Lee, M. L. Wahlqvist, *J. Nutr. Health Aging* **2011**, *15*, 815.
- [6] K. M. Davison, L. Gondara, B. J. Kaplan, *Nutrients* **2017**, *9*, 274.
- [7] M. A. Dualle, L. M. Robinette, I. E. Hatsu, *J. Immigr. Minor. Health* **2024**, *26*, 371.
- [8] P. Magesh, *IJO-International Journal of Social Science and Humanities Research (ISSN 2811-2466)* **2022**, *5*, 01.
- [9] J. J. Rucklidge, J. M. Johnstone, B. J. Kaplan, *Evidence-Based Practice in Child and Adolescent Mental Health* **2021**, *6*, 131.
- [10] I. Y. Fakolujo, O. M. Gbadeyan, F. A. Ibrahim, J. O. Oladele, A. T. Oladiji, in *Nutrition and Diet in Health*, CRC Press, **2024**, pp. 169–180.
- [11] G. Ede, *Change Your Diet, Change Your Mind: A Powerful Plan to Improve Mood, Overcome Anxiety, and Protect Memory for a Lifetime of Optimal Mental Health*, Balance, **2024**.
- [12] F. Zhou, Z. Ma, A. K. Rashwan, M. B. Khaskheli, W. A. Abdelrady, N. S. Abdelyaty, S. M. Hassan Askri, P. Zhao, W. Chen, I. H. Shamsi, *Foods* **2024**, *13*, 1610.
- [13] R. Haider, A. Mehdi, *Int. J. Integr. Sci.* **2024**, *3*, 69.

- [14] D. Sandua, *MIND-BODY CONNECTION: THE IMPACT OF NUTRITION ON MENTAL HEALTH*, 2023.
- [15] C. Singh, N. Yadav, K. Rao, N. Bansal, K. Archna, et al., *Curr. Nutr. Food Sci.* **2024**, 20, 966.
- [16] U. U. Ekpo, U. E. Umana, A. A. Sadeeq, *J Neuro Behav Sci.* **2023**, 10, 86.
- [17] B. R. Rane, R. R. Patil, A. S. Jain, R. K. Keservani, R. K. Kesharwani, in *Nutraceuticals and Functional Foods in Immunomodulators*, Springer, 2023, pp. 155–192.
- [18] J. Gea, A. Sancho-Muñoz, R. Chalela, *J Thorac Dis* **2018**, 10, S1332.
- [19] M. Kumar, D. Kumar, A. Sharma, S. Bhaduria, A. Thakur, A. Bhatia, *Curr. Nutr. Food Sci.* **2024**, 20, 62.
- [20] H. E. Babikir, P. Singh, *Clin Child Neurol.* **2020**, 483.
- [21] F. Anatolitou, *Journal of Pediatric and Neonatal Individualized Medicine (JPNIM)* **2012**, 1, 11.
- [22] D. I. Paduraru, *Journal of Mind and Medical Sciences* **2018**, 5, 151.
- [23] A. K. Leung, R. S. Sauve, *J. Natl. Med. Assoc.* **2005**, 97, 1010.
- [24] M. Zhang, H. Qiao, S. Yang, L.-Y. Kwok, H. Zhang, W. Zhang, *J. Agric. Food Chem.* **2024**.
- [25] G. Menon, T. C. Williams, *Arch. Dis. Child. Fetal Neonatal Ed.* **2013**, 98, F559.
- [26] C. M. Dieterich, J. P. Felice, E. O'Sullivan, K. M. Rasmussen, *Pediatr. Clin.* **2013**, 60, 31.
- [27] A. S. Cheema, L. F. Stinson, A. Rea, C. T. Lai, M. S. Payne, K. Murray, D. T. Geddes, Z. Gridneva, *Nutrients* **2021**, 13, 3724.
- [28] E. J. Filatava, C. E. Shelly, N. E. Overton, M. Gregas, R. Glynn, K. E. Gregory, *J. Perinatol.* **2023**, 43, 60.
- [29] E. L. Ford, M. A. Underwood, J. B. German, *Front. Nutr.* **2020**, 7, 54.
- [30] S. M. Innis, *Am. J. Clin. Nutr.* **2014**, 99, 734S.
- [31] FDA permits marketing of a diagnostic test to aid in measuring nutrients in breast milk, <https://www.fda.gov/news-events/press-announcements/fda-permits-marketing-diagnostic-test-aid-measuring-nutrients-breast-milk>, (accessed: May 2024).
- [32] M. T. Perrin, J. Festival, S. Starks, L. Mondeaux, E. A. Brownell, A. Vickers, *Current Developments in Nutrition* **2019**, 3, nzz116.
- [33] Lactationlab, <https://lactationlab.com/>, (accessed: May 2024).
- [34] Milkify, Nutritional Analysis, <https://milkify.me/products/nutritional-analysis>, (accessed: July 2024).
- [35] J. A. Mennella, C. J. Gerrish, *Pediatrics* **1998**, 101, e2.
- [36] K. E. Schaffer, C. D. Chambers, R. S. Garfein, W. Wertelecki, G. Bandoli, *Pediatr. Res.* **2024**, 95, 819.
- [37] UpSpring, Milkscreen, <https://myupspring.com/products/milkscreen?bvstate=pg:2/ctr>, (accessed: July 2024).
- [38] Frida, Breastmilk Alcohol Detection Test Strips, <https://frida.com/products/breastmilk-alcohol-detection-test-strips>, (accessed: July 2024).
- [39] J. Kulski, P. Hartmann, *Aust. J. Exp. Biol. Med. Sci.* **1981**, 59, 101.
- [40] Y. Lin, M. Bariya, A. Javey, *Adv. Funct. Mater.* **2021**, 31, 2008087.
- [41] B. Zhang, J. Lei, D. Qi, Z. Liu, Y. Wang, G. Xiao, J. Wu, W. Zhang, F. Huo, X. Chen, *Adv. Funct. Mater.* **2018**, 28, 1801683.
- [42] D. Nahavandi, R. Alizadehsani, A. Khosravi, U. R. Acharya, *Comput. Methods Programs Biomed.* **2022**, 213, 106541.
- [43] M. Seçkin, A. Ç. Seçkin, Ç. Gençer, *Biomedical Materials & Devices* **2023**, 1, 443.
- [44] J. K. Sommer, in *Smart Clothes and Wearable Technology*, Elsevier, 2023, pp. 67–80.
- [45] C. Wang, E. Shirzaei Sani, W. Gao, *Adv. Funct. Mater.* **2022**, 32, 2111022.
- [46] M. A. A. Mamun, M. R. Yuce, *Adv. Funct. Mater.* **2020**, 30, 2005703.
- [47] M. S. Kim, Y. Lee, J. Ahn, S. Kim, K. Kang, H. Lim, B.-S. Bae, I. Park, *Adv. Funct. Mater.* **2023**, 33, 2208792.
- [48] M. A. Lee, M. Song, H. Bessette, M. R. Davis, T. E. Tyner, A. Reid, *Int. J. Med. Inf.* **2023**, 105218.
- [49] W. Honda, S. Harada, T. Arie, S. Akita, K. Takei, *Adv. Funct. Mater.* **2014**, 24, 3299.
- [50] R. Furlan de Oliveira, P. A. Livio, V. Montes-García, S. Ippolito, M. Eredia, P. Fanjul-Bolado, M. B. Gonzalez Garcia, S. Casalini, P. Samorì, *Adv. Funct. Mater.* **2019**, 29, 1905375.
- [51] Y. Chu, J. Zhong, H. Liu, Y. Ma, N. Liu, Y. Song, J. Liang, Z. Shao, Y. Sun, Y. Dong, X. Wang, L. Lin, *Adv. Funct. Mater.* **2018**, 28, 1803413.
- [52] T. Yimyai, D. Crespy, A. Pena-Francesch, *Adv. Funct. Mater.* **2023**, 33, 2213717.
- [53] J. Yi, Y. Xianyu, *Adv. Funct. Mater.* **2022**, 32, 2113012.
- [54] S. M. Iqbal, I. Mahgoub, E. Du, M. A. Leavitt, W. Asghar, *npj Flexible Electron.* **2021**, 5, 9.
- [55] M. D. Bartlett, E. J. Markvicka, C. Majidi, *Adv. Funct. Mater.* **2016**, 26, 8496.
- [56] A. Tricoli, N. Nasiri, S. De, *Adv. Funct. Mater.* **2017**, 27, 1605271.
- [57] X. Hu, Y. Chen, X. Wang, K. Jia, H. Zhang, Y. Wang, H. Chu, X. Zhong, M. Lin, P. Chen, et al., *Adv. Funct. Mater.* **2024**, 34, 2312897.
- [58] Y. Jiang, A. A. Trotsuk, S. Niu, D. Henn, K. Chen, C.-C. Shih, M. R. Larson, A. M. Mermin-Bunnell, S. Mittal, J.-C. Lai, et al., *Nat. Biotechnol.* **2023**, 41, 652.
- [59] C. Ye, M. Wang, J. Min, R. Y. Tay, H. Lukas, J. R. Sempionatto, J. Li, C. Xu, W. Gao, *Nat. Nanotechnol.* **2024**, 19, 330.
- [60] T. Arakawa, K. Tomoto, H. Nitta, K. Toma, S. Takeuchi, T. Sekita, S. Minakuchi, K. Mitsubayashi, *Anal. Chem.* **2020**, 92, 12201.
- [61] J. R. Walter, S. Xu, J. A. Rogers, *Nat. Commun.* **2024**, 15, 123.
- [62] S. Mishra, Y.-S. Kim, J. Intarasirisawat, Y.-T. Kwon, Y. Lee, M. Mahmood, H.-R. Lim, R. Herbert, K. J. Yu, C. S. Ang, et al., *Sci. Adv.* **2020**, 6, eaay1729.
- [63] C. Cui, Q. Fu, L. Meng, S. Hao, R. Dai, J. Yang, *ACS Appl. Bio Mater.* **2020**, 4, 85.
- [64] K. Sel, D. Osman, N. Huerta, A. Edgar, R. I. Pettigrew, R. Jafari, *npj Digital Medicine* **2023**, 6, 59.
- [65] J. Tu, R. M. Torrente-Rodríguez, M. Wang, W. Gao, *Adv. Funct. Mater.* **2020**, 30, 1906713.
- [66] C. Ma, M.-G. Ma, C. Si, X.-X. Ji, P. Wan, *Adv. Funct. Mater.* **2021**, 31, 2009524.
- [67] J. M. Morse, J. L. Bottorff, *J. Nurse Midwifery* **1989**, 34, 15.
- [68] Little Lamb, Are reusable breast pads worth using?, <https://littlelamb.com/blogs/littlelamb-blog/are-reusable-breast-pads-worth-using>, (accessed: July 2024).
- [69] The Bump, Soaking through nursing pads, <https://forums.thebump.com/discussion/3382890/soaking-through-nursing-pads>, (accessed: July 2024).
- [70] Lansinoh, Stay dry disposable nursing pads, <https://lansinoh.com/products/stay-dry-disposable-nursing-pads>, (accessed: July 2024).
- [71] K. Promsawan, A. Soleh, K. Samoson, K. Saisahas, S. Wangchuk, J. Saichanapan, P. Kanatharana, P. Thavarungkul, W. Limbut, *Talanta* **2023**, 256, 124266.
- [72] Z. Zhao, H. Jiang, *Biosensors* **2010**, 302, 1.
- [73] Z.-D. Gao, Y. Qu, T. Li, N. K. Shrestha, Y.-Y. Song, *Sci. Rep.* **2014**, 4, 6891.
- [74] B. Bucur, C. Purcarea, S. Andreeșcu, A. Vasilescu, *Sensors* **2021**, 21, 3038.
- [75] P. Barathi, B. Thirumalraj, S.-M. Chen, S. Angaiah, *Microchem. J.* **2019**, 147, 848.
- [76] P. J. Rozance, J. I. Wolfsdorf, *Pediatr. Clin.* **2019**, 66, 333.
- [77] A. S. Cheema, L. F. Stinson, A. Rea, C. T. Lai, M. S. Payne, K. Murray, D. T. Geddes, Z. Gridneva, *Nutrients* **2021**, 13, 3724.
- [78] A. Suman, B. Mallory, H. Sybil L, R.-S. Carmen, S. Julian E, P. Barbara C, S. Barbara G, *Food Nutr. Sci.* **2011**, 2011.
- [79] M.-F. Tsoi, H.-L. Li, Q. Feng, C.-L. Cheung, T. T. Cheung, B. M. Cheung, *Obes Facts* **2022**, 15, 560.
- [80] R. Bromiker, A. Perry, Y. Kasirer, S. Einav, G. Klinger, F. Levy-Khademi, *J. Matern. Fetal Neonatal Med.* **2019**, 32, 786.

- [81] M. O'Brien, C. Gilchrist, L. Sadler, J. E. Hegarty, J. M. Alsweiler, *JAMA Pediatrics* **2023**.
- [82] U. M. Schaefer-Graf, R. Rossi, C. Bührer, G. Siebert, S. L. Kjos, J. W. Dudenhausen, K. Vetter, *Am. J. Obstet. Gynecol.* **2002**, 187, 913.
- [83] A. Thompson-Branch, T. Havranek, *Pediatr. Rev.* **2017**, 38, 147.
- [84] F. Amirghasemi, S. K. Nejad, R. Chen, A. Soleimani, V. Ong, N. Shroff, T. Eftekhar, K. Ushijima, A. Ainla, S. Siegel, et al., *Adv. Healthcare Mater.* **2024**, 2304122.
- [85] A. Al-Shami, F. Amirghasemi, A. Soleimani, S. Khazaee Nejad, V. Ong, A. Berkmen, A. Ainla, M. P. Mousavi, *Small* **2024**, 2311745.
- [86] J. Lin, Z. Peng, Y. Liu, F. Ruiz-Zepeda, R. Ye, E. L. Samuel, M. J. Yacaman, B. I. Yakobson, J. M. Tour, *Nat. Commun.* **2014**, 5, 5714.
- [87] S. K. Nejad, H. Ma, A. Al-Shami, A. Soleimani, M. A. Mohamed, P. Dankwah, H. J. Lee, M. P. Mousavi, *Sensors & Diagnostics* **2024**.
- [88] R. M. Torrente-Rodríguez, H. Lukas, J. Tu, J. Min, Y. Yang, C. Xu, H. B. Rossiter, W. Gao, *Matter* **2020**, 3, 1981.
- [89] A. Soleimani, F. Amirghasemi, A. Al-Shami, S. K. Nejad, A. Tsung, Y. Wang, S. L. Galindo, D. Parvin, A. Olson, A. Avishai, et al., *Biosens. Bioelectron.* **2024**, 259, 116321.
- [90] F. Amirghasemi, A. Al-Shami, K. Ushijima, M. P. Mousavi, *ACS Mater. Lett.* **2024**, 6, 4158.
- [91] R. R. Soares, R. G. Hjort, C. C. Pola, K. Parate, E. L. Reis, N. F. Soares, E. S. McLamore, J. C. Claussen, C. L. Gomes, *ACS Sens.* **2020**, 5, 1900.
- [92] N. T. Garland, E. S. McLamore, N. D. Cavallaro, D. Mendivelso-Perez, E. A. Smith, D. Jing, J. C. Claussen, *ACS Appl. Mater. Interfaces* **2018**, 10, 39124.
- [93] J. R. Sempionatto, M. Lin, L. Yin, E. De La Paz, K. Pei, T. Sonsa-Ard, A. N. de Loyola Silva, A. A. Khorshed, F. Zhang, N. Tostado, et al., *Nat. Biomed. Eng.* **2021**, 5, 737.
- [94] S. Khumngern, I. Jeerapan, *Commun. Mater.* **2024**, 5, 135.
- [95] R. Shiawku, H. Matsui, K. Nagamine, M. Uematsu, T. Mano, Y. Maruyama, A. Nomura, K. Tsuchiya, K. Hayasaka, Y. Takeda, et al., *Sci. Rep.* **2018**, 8, 6368.
- [96] R. Barber, J. Davis, P. Papakonstantinou, *ACS Appl. Nano Mater.* **2023**, 6, 10290.
- [97] L. Chao, W. Wang, M. Dai, Y. Ma, L. Sun, X. Qin, Q. Xie, *J. Electroanal. Chem.* **2016**, 778, 66.
- [98] F. Ricci, G. Palleschi, *Biosens. Bioelectron.* **2005**, 21, 389.
- [99] T. A. Matias, L. V. de Faria, R. G. Rocha, M. N. Silva, E. Nossol, E. M. Richter, R. A. Mu noz, *Microchim. Acta* **2022**, 189, 188.
- [100] K. Muzyka, G. Xu, *Electroanalysis* **2022**, 34, 574.
- [101] Y. Bleu, F. Bourquard, A.-S. Loir, V. Barnier, F. Garrelie, C. Donnet, *J. Raman Spectrosc.* **2019**, 50, 1630.
- [102] A. M. Farah, N. D. Shooto, F. T. Thema, J. S. Modise, E. D. Dikio, *Int. J. Electrochem. Sci.* **2012**, 7, 4302.
- [103] S. Nappini, A. Matruglio, D. Naumenko, S. Dal Zilio, M. Lazzarino, F. M. De Groot, C. Kocabas, O. Balci, E. Magnano, *J. Phys. Chem. C* **2017**, 121, 22225.
- [104] G. Moretti, C. Gervais, *J. Raman Spectrosc.* **2018**, 49, 1198.
- [105] P. Lazar, R. Mach, M. Otyepka, *J. Phys. Chem. C* **2019**, 123, 10695.
- [106] T. Kondo, D. Guo, T. Shikano, T. Suzuki, M. Sakurai, S. Okada, J. Nakamura, *Sci. Rep.* **2015**, 5, 16412.
- [107] J. Wang, Y. Qiu, D. Li, X. Liu, C. Jiang, L. Huang, H. Wen, J. Hu, *Microchim. Acta* **2019**, 186, 1.
- [108] A. Izadyar, M. N. Van, K. A. Rodriguez, I. Seok, E. E. Hood, *J. Electroanal. Chem.* **2021**, 895, 115387.
- [109] Y.-Y. Li, X.-X. Ma, X.-Y. Song, L.-L. Ma, Y.-Y. Li, X. Meng, Y.-J. Chen, K.-X. Xu, A. A. Moosavi-Movahedi, B.-L. Xiao, et al., *Sensors* **2023**, 23, 3209.
- [110] R. V. Blasques, J. S. Stefano, J. R. Camargo, L. R. G. e Silva, L. C. Brazaca, B. C. Janegitz, *Sensors and Actuators Reports* **2022**, 4, 100118.
- [111] J. Wang, *Chem. Rev.* **2008**, 108, 814.
- [112] D. Ma, S. Chon, S. Cho, Y. Lee, M. Yoo, D. Kim, D. Y. Lee, J. K. Lim, *J. Electroanal. Chem.* **2020**, 876, 114720.
- [113] C. Kalinke, P. R. de Oliveira, L. H. Marcolino-Júnior, M. F. Bergamini, *Talanta* **2024**, 274, 126042.
- [114] X. T. Zheng, M. W. N. Leo, Y. Yu, S. C. L. Tan, N. Nadzri, W. P. Goh, C. Jiang, X. P. Ni, P. Wang, M. Zhao, et al., *Adv. Funct. Mater.* **2024**, 34, 2310121.
- [115] E. Nossol, A. J. Zarbin, *Adv. Funct. Mater.* **2009**, 19, 3980.
- [116] N. Zhu, S. Han, S. Gan, J. Ulstrup, Q. Chi, *Adv. Funct. Mater.* **2013**, 23, 5297.
- [117] S. Y. Kim, D. Y. Yi, *Clinical and experimental pediatrics* **2020**, 63, 301.
- [118] D. Garwolinska, J. Namiesnik, A. Kot-Wasik, W. Hewelt-Belka, *J. Agric. Food Chem.* **2018**, 66, 11881.
- [119] C. A. Butts, D. I. Hedderley, T. D. Herath, G. Paturi, S. Glyn-Jones, F. Wiens, B. Stahl, P. Gopal, *Nutrients* **2018**, 10, 1231.
- [120] Y. Bai, Q. Guo, J. Xiao, M. Zheng, D. Zhang, J. Yang, *Sens. Actuators, B* **2021**, 346, 130447.
- [121] W. Wang, Y. Xie, Y. Wang, H. Du, C. Xia, F. Tian, *Microchim. Acta* **2014**, 181, 381.